Insights into Excitons Confined to Nanoscale Systems: Electron–Hole Interaction, Binding Energy, and Photodissociation

Gregory D. Scholes*

Department of Chemistry, 80 St. George Street, Institute for Optical Sciences, and Centre for Quantum Information and Quantum Control, University of Toronto, Toronto, Ontario M5S 3H6, Canada

ABSTRACT The characteristics of nanoscale excitons—the primary excited states of nanoscale systems like conjugated polymers, molecular aggregates, carbon nanotubes, and nanocrystalline quantum dots—are examined through exploration of model systems. On the basis of a valence bond-type model, an intuition is developed for understanding and comparing nanoscale systems. In particular, electron– hole interactions are examined in detail, showing how and why they affect spectroscopy and properties such as binding energy. The relationship between the bound exciton states and the nanoscale analogue of free carriers (charge-transfer exciton states) is developed. It is shown why the electron and hole act as independent particles in this manifold of states. The outlook for the field is discussed on the basis of the picture developed in the paper, with an emphasis on exciton binding and photodissociation.

KEYWORDS: nanoscience · nanoscale · exciton · spectroscopy · charge transfer · optical properties · aggregate · excited states

As devices are being designed on ever diminishing length scales, it is increasingly important to understand how fundamental electronic processes occur on the nanoscale in materials such as single-walled carbon nanotubes (SWNTs), nanocrystalline quantum dots, and molecular aggregates formed by self-assembled chromophores. Some materials can be scaled down in size and behave in a similar fashion to well-understood bulk analogues. For example, certain semiconductor nanowires have been shown to be effective for charge transport.[1] Contrarily, it is commonly found that spectroscopy of nanoscale systems differs significantly from that of bulk materials. Indeed, photoexcitation of nanoscale materials produces fascinating examples of excited electronic states at the junction of free carriers and molecular excitations.[2] Applications of relevance include displays,[3] solar cells,[4] detectors,[5] lasers,[6] electro-optical components,[7] and sensors.[8] It is challenging to understand these fundamental photoprocesses and to compare the wide range of materials that are currently of interest owing to the different limiting cases of theory that are applied to these systems (*e.g.*, Frenkel *versus* Wannier–Mott limits). The goal of this paper is to develop an intuitive understanding of the relationships between optical absorption, quantum confinement, free carrier formation, and exciton binding.

Nanoscale excitons are formed as a result of interactions among subunits that make up the structure. Those subunits may be atoms, such as carbon atoms in a SWNT, or they can be molecules or molecular subunits, as is the case in aggregates, crystals, and macromolecules. A prototypical nanoscale exciton is therefore described as a delocalized excitation, perhaps involving charge transfer—or sharing of electron density—among constituent subunits of the system. It is further notable that the extended nature of the electronic states helps excitation and charges to disperse rapidly over long length scales. It is therefore not surprising that nanoscale excitons have great potential for interfacing optical properties such as absorption or emission of light to electrical input or output. Each exciton state is a ladder of levels, or a continuum (at zero temperature) if one or more dimensions of the system is infinite in size. Owing to the large number of subunits involved in excitation sharing, there are a great many electronic levels in each of these exciton manifolds. To gain some perspective on the number of levels, first consider the basic manifold of excited states that define the lowest electronic excitations in a model molecule (say, ethene) of a particular symmetry. There are three triplets and

*Address correspondence to gscholes@chem.utoronto.ca.

Received for review September 12, 2007 and accepted January 22, 2008.

Published online February 13, 2008.
10.1021/nn700179k CCC: $40.75

© 2008 American Chemical Society

one singlet state. Contrast this with a small nanoscale system like a 1000 atom SWNT. Here there are 3 million triplet states and one million singlet states! Similarly, the number of lowest-energy exciton states can be seen in the optical spectra of CdSe nanocrystals calculated by Wang and Zunger.[9] The challenge is to discover the essential features of such complex problems. A useful conceptual starting point is to compare the absorption spectrum of a nanoscale material to the high-energy (5–20 eV range) absorption region of a molecule, such as benzene. A series of absorption bands between bound states lie among and on top of Rydberg series and ionization continua.[10] A key observation is the vast increase in density of states at excitation energies higher than the lowest absorption features.[11] It will be discussed below how this small-molecule system is not so different in some ways than a large nanoscale system.

A core theme in the electronic structure of excitons is the relationship between electrons and holes in the excited-state wave functions. To understand key properties of nanoscale excitons such as relaxation, binding energy, and photodissociation, it is desirable (i) to delineate states where electrons and holes are bound *versus* those where they act as free carriers; (ii) to characterize the average electron–hole pair separation in the exciton wave functions; and (iii) to quantify the number of states, and their energy distribution, in an exciton band. In the present paper, a simple model is formulated whereby the exciton states are constructed explicitly from linear combinations of configurations denoting the various ways one can arrange an electron and a hole on the subunits that make up the structure. On the basis of this valence bond-type model, the connection between optical absorption and charge transfer becomes apparent. For example, an important property of nanoscale excitons is that intense optical absorption occurs to a small set of "bound" states. It will be shown how those bound states relate to states comprised of separated charges. This model is inspired by early theories for electronic excitations in organic crystals[12] and descriptions of excimers, simple complexes formed between two molecules in the excited state.[13,14] Recent work on organic polymers and films provides some contemporary context for the model.[15–23]

Electronic spectroscopy enables us to probe selectively the "bound" states found at the low-energy end of the exciton manifold. A lot of information can be extracted from spectroscopic studies of these states, including the size of the exciton, *via* singlet–triplet splitting,[2] superradiant emission rates,[24] or pump–probe spectroscopy.[25,26] On the other hand, elucidation of the properties of separated electrons and holes poses a considerable challenge. For instance, a great deal of controversy surrounds the mechanism and details of photoinduced charge separation and the related issue of the magnitude of the exciton binding energy in extended, low-dielectric, nanoscale systems like conjugated polymers and SWNTs.[27–38] An intuition for these properties of nanoscale excitons would aid the discovery of connections between structure and properties through the design and examination of a range of model systems.

Introduction to Nanoscale Excitons. Excitons are typically discussed in two limiting cases.[39] In the first limiting case, it is assumed that the electronic interaction between the subunits is large and is dominated by one-electron terms that are proportional to wave function overlap. Then molecular orbitals that are delocalized over the entire system are a good starting point for describing electronic states.[40] Photoexcitation introduces an electron into the conduction orbitals, leaving a "hole" in the valence orbitals. The essentially free motion of the resulting electron and hole leads to formation of a Wannier–Mott type of exciton, characterized by a weak mutual attraction of the electron and hole which are, on average, separated by several subunits.[41,42] The strength of the electron–hole attraction determines the "binding" of the lower energy, optically allowed states compared to the dense manifold of charge-transfer (CT) exciton states, as will be shown in a later section of this paper. In a common assumption, the electron and hole move under their mutual attraction in a dielectric continuum, and then the exciton energy levels are found as a series analogous to the Rydberg series. Such a model cannot capture details of bonding and structure. This first limit naturally converges to the free carrier limit, where the electron–hole attraction is negligible compared to thermal energies. Photoexcitation of a nanoscale exciton in such a limit efficiently produces charge carriers, which is how a typical semiconductor solar cell works.[43]

In the second limiting case, electronic excitation is delocalized over the subunits (usually molecules), but the electron and hole are together localized on individual subunits.[44] That situation arises when the subunits are separated from each other by ~5 Å or more, in which case sharing of electron density among subunits is negligibly small in magnitude.[45] In other words, the orbital overlap between molecules is small, owing to the exponential decay of wave function tails.[46] In terms of the theoretical model discussed in the Methods section, the transfer integrals (that move electrons and holes between subunits) are sufficiently small that they can be neglected. The starting point for describing Frenkel exciton states is the properties of individual subunits or molecules. Electronic coupling between the molecules—in this case long-range Coulomb integrals—delocalizes the excitation, but that often occurs in competition with localization due to exciton–vibration coupling or disorder.[2,47–51] Photoexcitation of Frenkel exciton states does not naturally lead to charge carrier formation.

As a more general conceptual introduction to excitons confined to nanoscale systems, let us first recall the electronic excited states of molecules. There are two kinds of electronic transitions found in the energy range of 10 000−100 000 cm^{-1}: those involving the promotion of a valence electron to a "normal" antibonding orbital, and those series of excitations to Rydberg orbitals found below the ionization threshold for the orbital in question. This background is summarized in Figure 1. The Rydberg orbitals are highly diffuse compared to "normal" virtual orbitals and tend to be located at a strikingly large distance from the atomic centers of the molecule. A characteristic of these electronic transitions, therefore, is that the excited electron is transferred away from the original valence orbital (or the hole). As an example, a Rydberg series in the benzene spectrum[52] highlights the substantial energetic cost of separating the electron and hole. For example, in the $3e_{2g} \rightarrow npe_{1u}$ series, the energy required to go from $n = 3$ to $n = 4$ is reported to be over 1 eV.

To a first approximation, excitons in nanoscale materials can be considered also as being characterized by two kinds of excitations, as shown in Figure 1b. Locally excited configurations are formed by valence-to-virtual orbital excitation for any subunit in the system (*i.e.*, the electron and hole remain associated with the same subunit). Charge-transfer configurations are akin to the Rydberg excitations such that the electron is excited from one subunit to another with an associated energetic penalty. Continuing the analogy to a Rydberg series, there are a series of these configurations, depending on the electron–hole separation, that converge to the ionization threshold of an exciton in an infinitely large system, whereby free carriers are formed. But notice the use of *configurations* rather than *states*. That is because these configurations mix by electronic coupling to form the exciton states, and this is a key feature of exciton states that has considerable bearing on the topics under investigation in the present work. For example, mixing of the levels in the Rydberg-type series of charge-transfer configurations leads to a substantial lowering of the threshold for free carrier formation (*i.e.*, it does *not* then correspond to the ionization threshold at the convergence of the series).

Figure 1c shows a schematic picture of the electronic levels of a nanoscale system that results after mixing of the configurations introduced above. Each exciton band can be considered to be roughly divided into two parts. The lower ladder of states are the bound excitons, those wave functions where the electron and hole are close enough that their mutual attraction lowers the energy of the state relative to the dense band of charge-transfer exciton (CTX) states at higher energies. The vast majority of the exciton density of states can be attributed to the CTX states ($n^2 - n$ of the total of n^2 states, where n is the number of subunits). The CTX states are formed by strong mixing between configurations composed of widely separated electrons and holes. As will be explained later in this paper, a series of discrete states like the Rydberg series is not found because the electronic coupling between charge-transfer configurations outweighs their energetic separations. It will also be explained that, as a consequence, these CTX states have the properties of free carriers in the

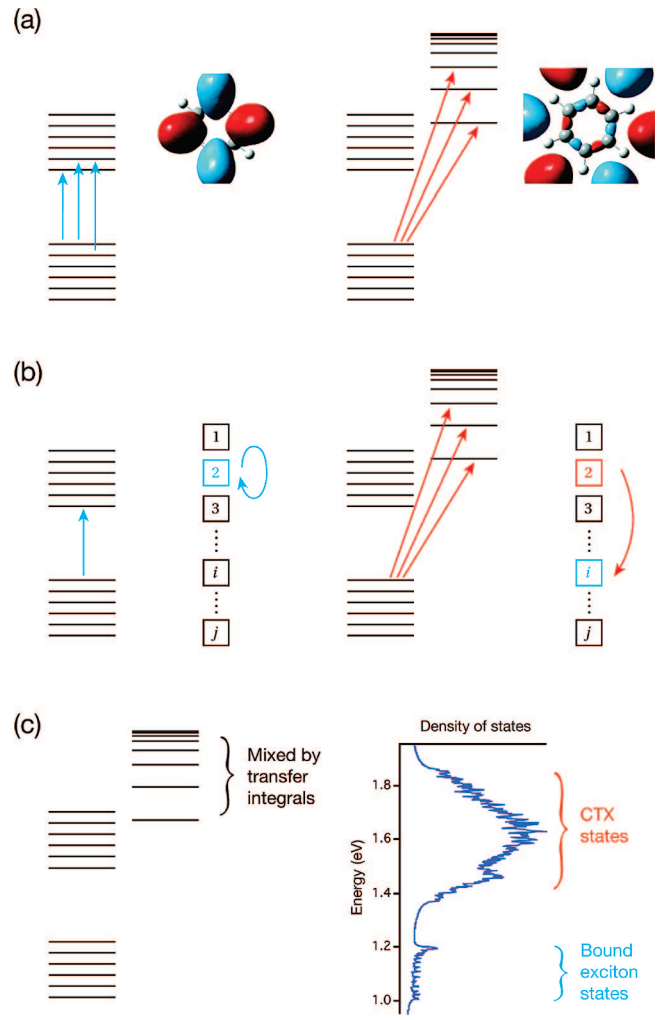

Figure 1. (a) There are two kinds of electronic excitations in molecules. The first type are those where valence electrons are excited to bound antibonding orbitals, where the excited electron is confined close to the hole (as in the representative orbital that is plotted). The second kind of excitation takes the electron away from the valence hole into one of a series of Rydberg orbitals (see representative orbital). This series converges to the ionization energy for the valence orbital. There is a substantial energetic cost associated with separating the electron and hole. (b) An analogy may be drawn with nanoscale excitons. Bound exciton states derive predominantly from excitation localized on or near constituent subunits of the material, whereas the nanoscale free carriers (charge transfer exciton, or CTX, states) involve excitation from one subunit to another, relatively distant, subunit. (c) A characteristic of exciton states is that, unlike the Rydberg states of molecules, the progression of sharp CT levels shown in part (b) is not seen. That is because the closely spaced levels are mixed by the transfer integrals that promote hopping of electrons and holes from one subunit to another. The resulting density of states is plotted, showing the ladder of lower levels, the bound exciton states that are associated with light absorption and emission, and the dense manifold of upper levels called the CTX states, wherein the electron and hole behave as independent particles.

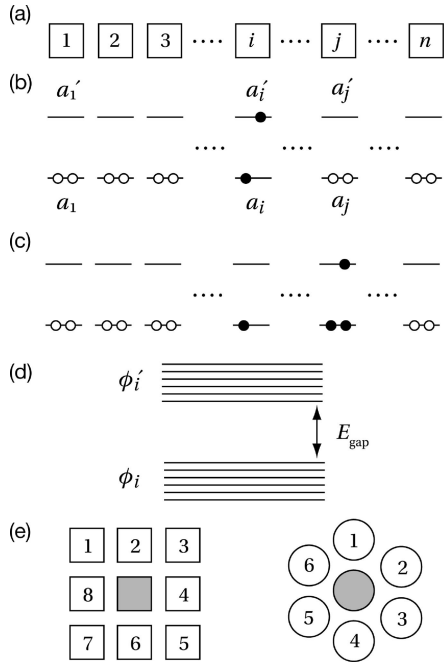

Figure 2. (a) The *n* subunits of a model nanoscale system arranged in a linear chain. (b) Locally excited configurations shown in terms of the highest occupied orbitals (a_i) and lowest unoccupied orbitals (a_i') of each subunit. (c) The analogous charge-transfer configurations. (d) The delocalized representation for orbitals of the model system showing the definition of the band gap. (e) Dimensionality increases the number of nearest-neighbor interactions. Two configurations of subunits for a two-dimensional system are shown, indicating the number of nearest-neighbor electron or hole acceptors for the central unit.

bulk—the electron and hole act independently—because the electron–hole attraction is much smaller than the transfer integrals that promote hopping of electrons and holes from one subunit to another.

Connections between Excitation and Charge Transfer. To understand the interplay between optical absorption and charge separation and to understand better the exciton binding energy, it is desirable to have a model that interpolates from the Frenkel limit, thus capturing the essential features of optical absorption, to the Wannier–Mott limit, in order to account for electron–hole separation. A similar concept has been recognized in the field of molecular crystals.[53] In the approach adopted here, an entire set of locally excited (LE) and charge-transfer (CT) basis configurations are considered in the context of a localized basis.[12] Such a method originates from valence bond theory,[54–57] and although it is a challenging method for large systems because of the number of structures needing to be considered and the nonorthogonality problem, it seems to be particularly useful for treating on equal footing high- and low-dielectric-constant nanoscale systems and has great pedagogical value.

The LE and CT configurations for a model linear aggregate are enumerated in Figure 2. This formulation of the system is easily associated with molecular aggregates: any system where the subunits retain a distinct identity and are not chemically bonded to each other. Of course, many nanoscale systems of interest are constructed by bonding networks (*e.g.*, SWNTs, nanocrystals), and it is not immediately apparent how the configurations of Figure 2 relate to these kinds of problems. It can be demonstrated that the basic model does hold, even when the subunits are bonded, as described in the Appendix and discussed in another context elsewhere.[58] The results are isomorphic to the formulation employed here, so the concepts highlighted in the present article are quite general.

Support for this kind of model, where local excitations mix with more separated electron–hole pair configurations, comes from electroabsorption measurements.[59,60] Analysis of electroabsorption data can reveal the interplay in the absorption spectrum of LE and CT configurations, particularly when they are weakly mixed, and thus is perhaps the most direct probe of the exciton manifold. Exciton states containing significant weights of CT configurations are known as charge-transfer excitons (CTXs). They play an important intermediate function in photoconduction or photogeneration of charge carriers[23,61–63] and a more subtle role in modifying the lower-energy absorption features of molecular crystals.[64] In nanoscale systems, there are often no true free carrier states—depending on the physical size of the system compared to the electron and hole Bohr radii—so CTXs can be the dominant excited electronic states. The CTXs carry negligible oscillator strength, *vide infra*, and form a dense manifold of states lying higher in energy than the bound exciton states. The significance of CTXs in nanoscale systems can be adjudged by their quantity: for *n* subunits in the system, there are *n* essentially neutral exciton states, but there are a stunning ($n^2 - n$) CTX states.

Definition and Implications of Electron–Hole Attraction. The energy of the CT configurations is controlled relative to the LE configurations (see Methods) by the electron–hole separation according to the empirical expression[65,66] (eq 1),

$$C_{ij} = \frac{C_0}{\epsilon_{\text{static}}\sqrt{1 + \eta R_{ij}^{\ 2}}} \tag{1}$$

where ϵ_{static} is the static (zero-frequency) dielectric constant of the medium. This empirical equation is often used in semiemprical calculations, where the value of η is chosen to ensure the best agreement between the calculations and experiment. There is no rigorous justification for this equation. The main features of eq 1 are that it ensures that the integral $(aa|bb)$ converges to $(aa|aa)$ when $R_{ij} = 0$, and otherwise decreases with the inverse of R_{ij}, as expected for a Coulombic interaction between point charges.

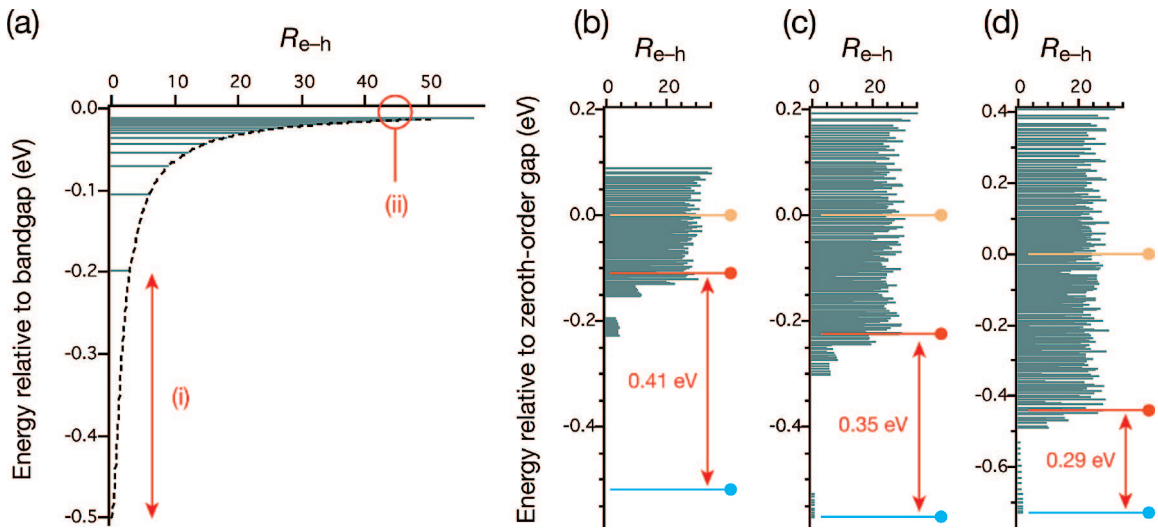

Figure 3. Eigenvalues calculated for a model system consisting of 20 subunits spaced by 3 Å. In each calculation, $C_0/\epsilon_{static} = 0.5$ eV. The relative energy of each eigenstate is plotted *versus* average electron–hole pair separation $R_{e\text{-}h}$ in the corresponding wave function. (a) The transfer integrals are set to zero so the configurations do not mix. It can be seen that as $R_{e\text{-}h}$ increases, the energy approaches that of the free (non-interacting) electron–hole pair (the zeroth-order gap). Panels (b), (c), and (d) show how model (a) changes when electrons are allowed to hop between sites (*via* the transfer integrals). Results of calculations using average transfer integrals of 28, 56, and 112 meV, respectively, are plotted. The transfer integrals strongly mix quasi-degenerate configurations to form a dense band of delocalized CTX states split above and below the zeroth-order gap (brown markers located at zero energy). The lowest-energy (blue) marker shows the energy of the lowest exciton state. The red marker shows the onset of the nanoscale free carrier states calculated by setting $C_{ij} = 0$ (*i.e.*, the band gap). The energy difference between the red and blue markers defines the exciton binding energy.

For the model calculations reported here, $\eta = 0.6$ is used, which is typical of values chosen for organic materials. To illustrate the role played by C_{ij} in determining the zeroth-order energies of the various electron–hole configurations, the transfer integrals are set equal to zero and the eigenstates are calculated for a model system consisting of 20 subunits spaced by 3 Å. The result for $C_0/\epsilon_{static} = 0.5$ eV is shown in Figure 3a. By plotting the relative energy of each eigenstate *versus* average electron–hole pair separation $R_{e\text{-}h}$ in the corresponding wave function (eq 9, below), it can be seen that as $R_{e\text{-}h}$ increases, the energy approaches that of the free (non-interacting) electron–hole pair (the zeroth-order gap). The energy lowering of the upper zeroth-order CT configurations compared to the free electron and hole, indicated by (ii) in Figure 3a, is caused by the finite size of the system. Note also that the spacing between consecutive eigenstates diminishes as $R_{e\text{-}h}$ increases. These trends are determined by the lattice spacing between subunits, the magnitude of C_0, and the static dielectric constant of the medium. For comparison, $C_{ij}(R)$ is plotted as the dashed line, and the energy difference between the lowest- and next-lowest-energy states is indicated as (i) in Figure 3a.

When C_0 is large (*e.g.*, often it is chosen to be 1.0 eV or higher for organic materials) and the static dielectric constant ϵ_{static} is small, it is seen that there can be a substantial energetic difference between closely associated and well-separated electron–hole configurations. As noted in the Methods section, only those configurations that contain very closely associated electron–hole pairs contribute to the transition dipole of each eigenstate,[67] which explains why electronic absorption occurs only to a comparatively small number of exciton states that lie significantly lower in energy than the dense manifold of CTX states.[59,68]

In Figure 3b–d, plots are shown for average transfer integrals of 28, 56, and 112 meV, respectively. The transfer integrals strongly mix quasi-degenerate configurations (those spaced by a magnitude similar to the value of the transfer integral) to form a band of delocalized CTX states split above and below the zeroth-order gap (indicated by the topmost (brown) marker in each plot) by approximately 4 times the magnitude of the transfer integral.[69] That delocalization is signaled in the plots by these states all having approximately the same $R_{e\text{-}h}$ according to eq 9. Thus, the transfer integrals, which promote electron and hole hopping between subunits, act to overwhelm the electron–hole attraction C_{ij} in the band of CTX states, meaning that the electron and hole act as independent particles. Although the electron and hole are confined in the nanoscale system, they are "unbound", like free carriers in the bulk. It therefore makes sense that the band gap of the exciton, indicated by the middle (red) marker, lies at the bottom of this distinct band of CTX states. It was determined in each case as the lowest-energy eigenstate calculated with $C_{ij} = 0$. The band gap is dictated by the magnitude of the transfer integrals in conjunction with the form of the electron–hole attraction and lattice spacing. It is equivalent to the energy spacing between the highest occupied valence orbital and lowest-energy conduction orbital (Figure 2d).

The bound exciton states are those formed by configurations with zeroth-order energy gaps that are determined by the lowest-energy part of the C_{ij} potential; therefore, they consist of closely associated electrons and holes. Bands of states are formed through mixing of similar kinds of configurations by the transfer integrals. For example, the lowest two bands are indicated in Figure 3b at ~ -0.5 and -0.2 eV, little perturbed from the parent configurations shown in Figure 3a. The binding energy of the exciton at fixed nuclear configuration and zero temperature is indicated in Figure 3b–d as the energy difference from the band gap to the lowest-energy exciton state. The three "gaps" indicated in this figure are summarized as follows: (i) the zeroth-order gap, that is, the difference between ionization energy and electron affinity of a single subunit in the system; (ii) the band gap, which is the threshold for nanoscale free carrier generation; and (iii) the optical gap, which is the lowest-energy absorption threshold, populating a bound exciton state.

Size dependences of the exciton binding energies are expected and have been reported for various nanoscale systems, for example, quantum dots and SWNTs.[70,71] The binding energy at the level of calculation developed in this section depends on the magnitude of the transfer integrals and the form of C_{ij}. It also depends on the size of the nanoscale system *via* the size scaling of C_{ij}. That size scaling can easily be understood in the delocalized (molecular orbital) representation as the reduction in electron–hole attraction with delocalization of their wave functions (the average charge–charge separation diminishes as charge distribution becomes more diffuse). In the localized representation, this is understood as a diminished magnitude of the most attractive electron–hole configurations as those wave functions are mixed with greater numbers of more-separated electron–hole configurations, hence reducing their weight in the lowest-energy states. That dilution of the configuration weights can be significant when transfer integrals are appropriately large because, out of the total n^2 configurations, merely n configurations are the locally excited configurations and $(n - 1)$ are nearest-neighbor CT configurations, which together represent the lowest-energy configurations. Similarly, dimensionality plays an important role by increasing the number of nearest-neighbor transfer integrals at each site (Figure 2e). For example, in a close-packed sphere structure, each unit has two nearest neighbors in a 1D system, six nearest neighbors in a 2D system, and 12 nearest neighbors in a 3D system.

At this point, the reader may be wondering if the exciton should always be bound (at 0 K). This kind of question can really only be addressed using sophisticated calculations for each specific case, but evidence at present suggests that the lowest states are typically bound. There are two related examples that serve to strengthen this observation. First, in molecules, bound states are known to lie below the Rydberg states. Second, in valence bond studies, it is typical that the more extended ionic configurations are found to contribute with small weight to the wave functions of the lowest electronic states (see, *e.g.*, refs 72 and 73). In other words, in many molecular systems, the energetic cost of separating the electron and hole is significant compared to the transfer integrals. As a consequence, the lowest electronic states are bound. As an example, the conclusions described here can be tested for a strongly coupled molecular aggregate using the integrals obtained from *ab initio* calculations.[74]

Coulomb and Exchange Effects. In this section, Coulomb and exchange interactions, as defined in our localized representation, will be examined. In the usual delocalized representation, these effects are captured collectively as the exchange interaction that decides singlet–triplet splitting. In effective mass approximations, the exchange interaction is typically added perturbatively and then has short-range and long-range contributions[75] (similar to our J_0 and V^{Coul}). In the localized representation, the exchange interaction is primarily due to the term J_0 from eq 5a (below), which is the singlet–triplet splitting of subunit i in isolation. However, it is corrected by addition of the Coulombic interactions, V^{Coul}, that determines the way that singlet–triplet splitting depends on size, dimensionality, and perhaps even shape in appropriately designed systems.

Exchange effects are considered to be a small correction to the theory of excitons in high-dielectric-constant solid-state materials. However, because their magnitudes are dependent on the size of the nanoscale system,[2] their significance in QDs has been examined,[70] and it has been established that these effects are important for determining the fine structure of the lowest-energy states.[76,77] On the other hand, these kinds of interactions completely determine the Frenkel-type exciton states of most molecular materials.[47] Evidence suggests that Coulombic and exchange interactions are *together* typically significant in deciding the spectroscopic properties of nanoscale materials,[2] and especially the spectroscopy of the lowest-energy states, so a careful examination is warranted. Furthermore, these effects play an important role in deciding singlet *versus* triplet exciton yields in organic light-emitting devices.[15,78]

As reviewed recently, the singlet–triplet splitting is distinctly size-dependent for nanoscale materials.[2] The advantage of such a subtractive method in spectroscopic studies of excitons is that the band gap, which depends on one-electron energies, is subtracted away, leaving two-electron contributions to the excitation energies that can often be most illuminating. As an example, the size dependence of the excitation energy for the first excited singlet state of a series of polyacenes[79–81] is plotted in Figure 4. The systematic lowering of the excitation energy as a function of the

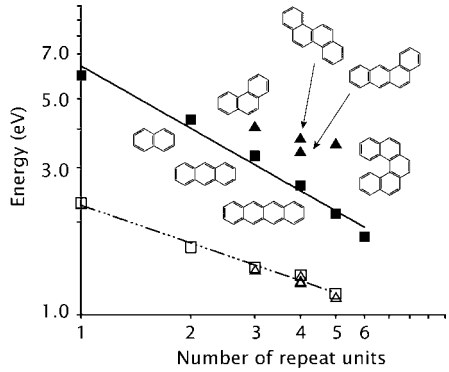

Figure 4. Filled symbols indicate the lowest-energy singlet state transition energy for each polyacene system. The squares denote linear polyacenes (benzene, naphthalene, anthracene, tetracene, and pentacene), while the triangles correspond to other ways of connecting the aromatic rings (phenanthrene, chrysene, 1,2-benzanthracene, and benz[*g*]chrysene). A clear correspondence between size and transition energy is found only for the homologous linear polyacene series. In contrast, singlet–triplet splitting (open symbols) probes the size of the excitation and evidently depends only on the number of aromatic rings, not on their precise spatial configuration.

number of rings in the linear polyacene series (square symbols) is evident, as expected.[79,82] However, consider the points plotted as triangular symbols. It is not merely the number of aromatic rings—or size—that determines the excitation energy, but clearly it matters precisely how the rings are organized. On the molecular length scale, structure has a significant influence on excitation energies through the orbital energies (band gap). Now consider the energy splitting between the first excited singlet and triplet states of the polyacene molecules, also plotted in Figure 4 (open symbols). It is apparent that shape is inconsequential, and only the total number of repeat units tunes that splitting, thus providing a signature of exciton size in molecules through the size-scaling of singlet–triplet splitting, which is evidently weakly dependent on shape for these molecules.

One way to think about the size dependence of the exchange interaction is that the repulsion between the transition densities, describing excitation from delocalized valence orbital *v* to delocalized conduction orbital *c*, diminishes concomitant with the increasing average size of the transition charge distribution because of an increasing average separation between charges. That is the same idea as discussed above for the electron–hole attraction. However, it is also found that size dependence is derived from a correction to J_0 by the long-range Coulombic interaction, V^{Coul}, that originates from the matrix elements between different LE configurations.[83] This seems to be a satisfactory way of thinking about the scaling of the exchange interaction with size, and therefore properties like singlet–triplet splitting, because it allows a clear understanding of why long-range interactions are important in moderating the size-scaling.

The energy difference between the lowest singlet and lowest triplet eigenstates results from the ratio of the number of interactions possible to the square of the normalization factor. For a linear aggregate consisting of *n* units,

$$E_{S-T} \approx 2J_0 - \frac{2(n-1)J_1}{n} - \frac{2(n-2)J_2}{n} \ldots \qquad (2)$$

where J_1 is the Coulombic coupling between nearest-neighbor units, J_2 is the Coulombic coupling between next-nearest-neighbor units, and so on. Analogously, the result can be generalized to higher dimensions. If eq 2 is truncated at the nearest-neighbor Coulombic term, and we assume that J_1 is similar in magnitude to J_0 (a reasonable assumption only if the subunits are very close together), then the singlet–triplet splitting is $E_{S-T} \approx 2J_0/n$, scaling as $1/n$, as predicted from a particles-in-a-box model as well as more detailed models such as in the work of Bittner and Karabunarliev.[15] Notice that this is independent of the mixing between the LE and CT configurations and therefore applies also to Frenkel excitons. Owing to the weak attenuation of V^{Coul} with distance (roughly $1/R^3$), the size-scaling of the singlet–triplet splitting is actually substantially less severe than predicted by simple models.[2] Through inspection of eq 2, it is deduced that this amelioration of the size-scaling of the singlet–triplet splitting is due largely to the terms J_2, J_3, and so on.

In Figure 5a−c, the effect is shown of introducing the Coulombic interaction to the model calculations plotted in Figure 3b. The additional contribution to the exciton binding energy is indicated, and it is seen to depend on the magnitude of the Coulomb interaction. The sign of V^{Coul} can change the energy distribution of the lower manifold of states, but most importantly it decides whether the allowed absorption is to the lower or upper state in the exciton manifold (J- or H-aggregate). That is shown in Figure 5d,e, where absorption spectra and density of states are plotted. These spectra are calculated on the basis of the parameters of Figure 5, panels c and b, respectively. In the case of Figure 5d, optical absorption occurs into the lowest bound exciton state, and the onset of the density of CTX states is evident at around 1.4 eV. For the case of Figure 5e, absorption occurs to the upper bound exciton states, meaning that excitation will relax to the dark states at lower energy. This kind of nanoscale system is in principle non-fluorescent, but in practice fluorescence is usually observed.[37,38,84–88] The ways that the Coulombic interaction governs the distribution of allowed optical transitions based on organization of the subunits can provide clues to the structure.[89] This idea has not been exploited extensively in studies of nanoscale systems but may be rather useful for elucidating structural hierarchies of assemblies.

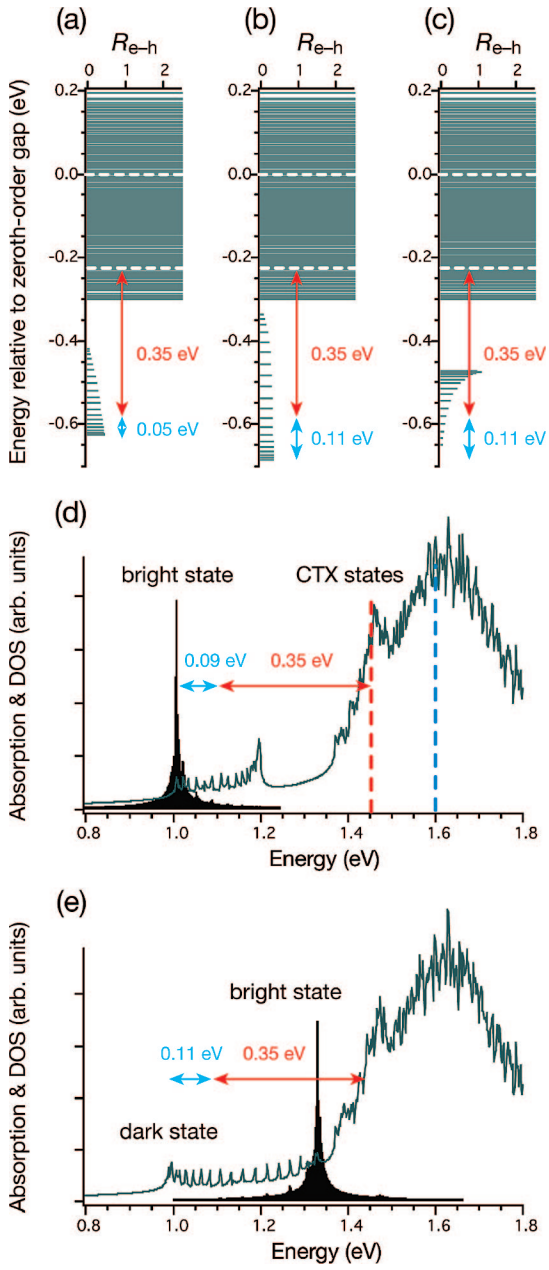

Figure 5. (a−c) Model calculations based on those plotted in Figure 3b, but with the addition of the Coulombic interaction. The electron-transfer integral is 500 cm^{-1}, and the hole-transfer integral is 400 cm^{-1} (overlap integrals set to 0.01). The nearest-neighbor and next-nearest-neighbor Coulombic interactions are respectively (a) 300 and 37 cm^{-1}, (b) 600 and 75 cm^{-1}, and (c) −600 and −75 cm^{-1}. The additional contribution to the exciton binding energy from the Coulombic interaction is indicated by the blue arrow. The total binding energy is given by the sum of the blue and red arrows. (d) Absorption spectrum (solid black band) and density of states (charcoal line) calculated for the parameters from part (c), with the excitation energy gap set to 2 eV. The blue dashed line indicates the zeroth-order gap, while the red dashed line shows the onset of the CTX "free carrier" density of states (*i.e.*, the band gap). (e) Absorption spectrum (solid black band) and density of states (charcoal line) calculated for the parameters from part (b).

The Frenkel limit is obtained when C_0 is significantly greater in magnitude than the transfer integrals. Hence, it is typical when the subunits are well-separated and the dielectric screening is small. In that limit, the CT configurations can be neglected since they mix negligibly with the LE configurations and their eigenstates lie at considerably higher energies.

As a final point, it is noted that the Coulombic interaction is screened (reduced in magnitude) by the optical dielectric constant of the medium. A complication is that the screening depends on shape, size, and separation of the subunits. On the basis of quantum chemical calculations, recent work suggests that interactions between proximate molecular subunits can be essentially unscreened, and the screening is introduced exponentially with subunit separation.[90] Other work predicts that the effective dielectric constants of quantum dots may be significantly reduced relative to bulk values.[91] Understanding these dielectric effects is an important topic for future work.

Nanoscale Excitons and Photodissociation. The electron and hole behave as independent particles in the manifold of CTX states. The condition for independent electron and hole is that the transfer integral is greater than the electron–hole attraction for the configurations that make up the (CTX) eigenstate. Then the propensity for electron or hole to hop is greater than their mutual attraction. By definition, the above condition does not hold for the bound exciton states, although this point is sometimes overlooked. It is therefore incorrect, for example, to assert that optically bright nanocrystal states are comprised of unbound electron–hole pairs. Indeed, the binding energies of excitons in QDs have been established to be several tens of millielectronvolts,[70] which is not much less than those of conjugated polymer chains[27] and SWNTs.[34]

To overcome the binding energy, photodissociation of an exciton can occur by thermal activation.[92] In the extreme case where sufficiently high dielectric screening causes the CTX configurations to be within *kT* of the LE configurations, photoexcitation leads to very efficient formation of free carriers, as in bulk inorganic semiconductors. A possible mechanism at work in low-dielectric materials is coupling of higher-energy electronic transitions to resonant CTX states derived from a lower exciton state. That coupling can provide oscillator strength for the CTX states, enabling excitation-wavelength-dependent photodissociation.[63]

A characteristic of some nanoscale materials is energetic disorder. As an example of the implications of this disorder, the calculations presented in Figure 3 will be repeated for the situation where this model aggregate mimics, for example, a lamella domain in a conjugated polymer film.[93,94] In that situation, the model for the perfect system, such as considered above, is modified by the introduction of significant disorder in the band gap of each subunit. That disorder can arise from variations in the local environment in addition to the presence of conformational disorder on the polymer chain, leading to conjugation breaks.[95–98] Each subunit in the

calculation then represents a conformational subunit. The aggregate Hamiltonian is comprised of interchain interactions within an array of these conformational subunits. In order to maintain consistency, we use the same Hamiltonian and parameters as in the previous section of this paper.

The disorder was introduced into the calculations by adding an offset Δ_{ij} to the site energies (eqs 5a and 5b, below), as has been done in the past for Frenkel excitons.[47] Here that approach is extended to general excitons; consequently, the notation Δ_{ij} refers to the configuration where there is a hole at site *i* and an electron at site *j*. Off-diagonal disorder was neglected. Two instances of disorder are identified: disorder in the electronic excitation energies Δ_{ii}, and disorder in the energies of the CT configurations Δ_{ij}. The Δ_{ii} are considered to be smaller on average than Δ_{ij} owing to the correlation between the fluctuations of electron and hole energies when they reside on the same subunit. Each offset is taken from a Gaussian distribution with standard deviation σ_{LE} or σ_{CT}, respectively. Owing to the way that quantum confinement effects alter the valence and conduction orbital energies symmetrically about the mean of the distribution, pairs of CT configurations should be almost perfectly anticorrelated: $\Delta_{ij} = -\Delta_{ji}$. That is assumed in these calculations. The interesting corollary of that assumption is that disorder breaks the symmetry of the CT resonance, meaning that individual eigenstates may have a dipole moment.

In Figure 6, some model calculations are shown. We see that the effect of disorder is to smear out the bound exciton states and the CTX states. When disorder is significant relative to the transfer integrals, the distinction between bound exciton states and CTX states is blurred, thus making the unequivocal definition of binding energy difficult. It can also be seen that the average electron–hole separation varies with energy across the CTX density of states. That derives from localization of the CT configurations.

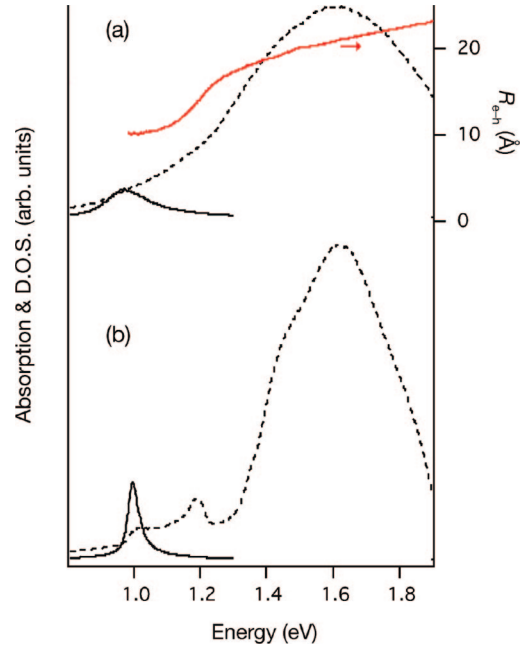

Figure 6. Absorption spectra (solid black lines) and densities of states (dashed lines) calculated using the parameters of the plot in Figure 5d but with the inclusion of disorder in the site energies (see text). The red line in the upper plot shows the average electron–hole separation in the density of states calculated using eq 9. The calculations were performed using a Monte-Carlo sampling over 2000 iterations. (a) $\sigma_{LE} = 750$ cm^{-1} and $\sigma_{CT} = 1500$ cm^{-1}. (b) $\sigma_{LE} = 250$ cm^{-1} and $\sigma_{CT} = 500$ cm^{-1}.

SUMMARY AND OUTLOOK

The article examined electronic states of excitons confined to model nanoscale systems, aiming to give the reader a sense of how to think about questions such as: What are the distinguishing features of nanoscale excitons and their properties? What properties are size-tunable and why? It was shown that a critical parameter in deciding the nature of the exciton states in a nanoscale system is the distance dependence of the electron–hole interaction, and the resulting series of energy states was likened to a Rydberg series. However, these configurations in the series mix, the result being a partitioning of the series of states into two manifolds: the bound excitons and the CTX states (confined free carriers).

The mixing among the series of configurations is instigated by transfer integrals that promote hopping of electrons and holes from one site to another (their magnitude is determined largely by center-to-center separations of the subunits). The relative magnitude of the transfer integrals compared to spacing between states in the ladder of CT configurations decides the extent of mixing. It was found that the closely separated electron–hole pair configurations dominated the lower-energy state composition because of the significance of electron–hole attraction in these configurations, and these states persisted as a ladder of bound exciton levels after mixing. On the other hand, configurations containing extended electron–hole pairs were found to be closely spaced in energy and were therefore strongly mixed by the transfer integrals, thus leading to formation of a dense manifold of CTX eigenstates.

The lowest-energy set of states, dominantly comprised of closely bound electron–hole pair configurations, were clearly distinguished from the abrupt onset of the vast number of CT states, thus defining the exciton binding energy with astonishing clarity. This picture led to the definition of free carriers confined to nanoscale materials. When the transfer integrals are greater than the separation between configuration energies, the electron and hole have a propensity to hop from one site to another rather than remaining bound by the electron–hole attraction. Thus, the electron and hole act as independent particles in the manifold of CTX states, providing the nanoscale analogue to free carriers.

The magnitude of the binding energy is decided by the screened electron–hole attraction in conjunction with the transfer integrals. The long-range Coulombic interaction (known as the exchange interaction in the molecular orbital representation) further binds the exciton. However, perhaps the most important role of this term is to distribute oscillator strength among the lowest-energy states according to structural parameters. Its significance is seen in the size-dependence of the singlet–triplet splitting, which can be traced back to this interaction. A further important facet of the exchange/Coulomb interaction is that it is responsible for determining the spin eigenstates, thus establishing the rules for spectroscopy. In the case of quantum dots, the spin–orbit coupling also plays a significant role in this regard.

It was shown that there are extraordinary numbers of exciton states in nanoscale materials, scaling as the square of the number of subunits. What are the implications of such a high number of excited states? Owing to the ladder of dark states rising above the lowest bright exciton state of SWNTs, the radiative rate depends on the partitioning of population among bright and dark levels of an exciton manifold, and hence on the temperature.[99] If the exciton binding energy is small, then thermal excitation can separate electron–hole pairs—possibly a desirable situation for solar energy conversion. Similar considerations apply to molecular aggregates, but with the additional complication that thermal excitation or relaxation processes occur concomitant with spatial transfer of bound excitons owing to the effects of disorder.[100] The enormous number of states in the exciton manifolds also differentiates the mechanism of relaxation processes in nanoscale materials, like QDs,[101,102] compared to molecules. Dimensionality is an important issue and is basically equivalent to considerations of molecular structure, as is described by the author elsewhere.

How charge carriers are formed after photoexcitation of conjugated polymers remains an open question.[30] The present article provides some intuitive insights, but the challenge is that the structure of conjugated polymer exciton states depends on the admixture of intrachain and interchain excitons. It has been established that interchain interactions are important for photogeneration of charge-transfer states in poly(3-hexylthiophene),[32] and it is known that the yield of charge carriers increases as excitation is tuned to higher energies above the lowest optically allowed transition.[16,31,33] A further complexity is conformational disorder of the polymer chains. By breaking the π-system into a distribution of conformational subunits, it is feasible that a more extensive admixture of LE and CT configurations might be possible (cf. Figure 6), but as yet the possible implications of structural complexity and disorder are unknown.

The key to efficient optical generation of free carriers is to design a system wherein the CT states lie close to, or even below, the optical transition (predominantly LE states).[103] That has been achieved by using polymer blends[104] and polymers mixed with electron acceptors,[105] though understanding better the properties of nanoscale excitons in such heterogeneous systems is a challenge for the future. Identifying the electronic states is just part of the problem, because exciton–phonon coupling plays a central role in determining the dynamics subsequent to photoexcitation.[106]

As a final note, the significance of dielectric screening of the electron–hole attraction and the Coulombic interactions is well-known, but how to quantify that screening remains a challenge. It is likely that size and surface effects reduce the screening in QDs significantly, and future work may shed more light on that issue. The magnitude and form of the screening in the rich π-electron systems of SWNTs also remain elusive. Again, it is likely that simple bulk screening prescriptions do not apply.

METHODS

In the calculations reported here, the LE and CT configurations were mixed by extending the theory introduced by Harcourt *et al.*[83] That is done by writing the Hamiltonian for a system consisting of n subunits in the block-diagonal form:

$$\mathbf{H} = \begin{bmatrix} \mathbf{H}_{LE} & \mathbf{H}_{LE-CT} \\ \mathbf{H}_{CT-LE} & \mathbf{H}_{CT} \end{bmatrix} \quad (3)$$

The top-left block of eq 3 has dimension n and contains the site energies of the LE configurations and the matrix elements between them. These matrix elements primarily involve the long-range Coulomb interaction, V^{Coul}. This Coulomb interaction is a coupling between transition densities of the subunits. This interaction is now well-understood and can be calculated accurately, as described elsewhere.[107–111] If the subunits are separated on the length scale of chemical bonds, then orbital overlap effects impart an important additional contribution to the electronic coupling matrix elements within the LE block.[45] The Frenkel exciton states are obtained in the limit when these orbital overlap effects are negligible by diagonalizing just the $\mathbf{H}_{LE}$ block.

The lower-right block of eq 3, $\mathbf{H}_{CT}$, has dimension $(n^2 - n)$ and contains the energies of the CT configurations—these are a function of the electron–hole separation—and the electronic coupling matrix elements that transfer electrons and holes spatially by the action of an electronic coupling known as the transfer integral.[83,112,113] Similar interactions mix the LE and CT blocks. In the Wannier–Mott model, only the CT block needs to be considered. The justification for neglecting the LE block is the overwhelming number of CT configurations compared to LE configurations, which will therefore dominate the eigenstate composition when the subunits are closely spaced and strongly interacting.

Spin-symmetry-adapted configuration state functions (CSFs) Ψ_r are constructed on the basis of the diagrams shown in Figure 2 and are written in eqs 4a and 4b. These serve as basis configurations to obtain the nanoscale exciton states.[54,114] Each CSF is an eigenfunction of the total spin operator S^2, as implied by the superscripts of S (singlet state with $S = 0$, $M_s = 0$) or T

(triplet state with $S = 1$, $M_s = 0$). To consider relativistic effects or fine structure such as zero-field splitting, all three triplet CSFs should be considered. A bar over a spin-orbital indicates that it contains an electron of spin β, while the unbarred spin-orbitals contain an electron of spin α.

$$^{S,T}\psi_{r=\{LE\}} \approx (|a_1\bar{a}_1a_2\bar{a}_2...a_i\bar{a}_i'...| \pm |...a_1\bar{a}_1a_2\bar{a}_2...a_i'\bar{a}_i...|)/\sqrt{2} \quad (4a)$$

$$^{S,T}\psi_{r=\{CT\}} \approx (|a_1\bar{a}_1...a_i\bar{a}_j'...a_j\bar{a}_j...| \pm |a_1\bar{a}_1...a_i'\bar{a}_j...a_j\bar{a}_j...|)/\sqrt{2} \quad (4b)$$

It is noted that spin–orbit coupling is significant in certain nanoscale systems, such as quantum dots. In that case the approach presented here can be appropriately modified.

The CSFs and the matrix elements were expanded up to first order in overlap, yielding expressions for the singlet and triplet LE and CT site energies in terms of one-electron integrals among localized orbitals, $h_{ab} = \langle a|h|b\rangle$, and two-electron integrals, $(ab|cd) = \langle a(1)c(2)|1/r_{12}|b(1)d(2)\rangle$. The result is

$$^{S,T}H_{LE}(i,i) \approx h_{i'i'}(\text{size}) - h_{ii}(\text{size}) + (a_i'\,a_i'\,|a_ia_i) - (a_ia_i|a_ia_i) \pm J_0^i - P_{LE}$$
$$= E_{LE}^i \pm J_0^i - P_{LE} \quad (5a)$$

$$^{S,T}H_{CT}(i,j) \approx h_{j'j'}(\text{size}) - h_{ii}(\text{size}) + C_0^j - C_{ij} - P_{CT}$$
$$= \text{IP}_i - \text{EA}_j - C_{ij} - P_{CT} \quad (5b)$$

These diagonal energies are written relative to the ground-state energy (E_0). The (i,j) label on the left-hand side of the equations means that the hole is at site i and the electron is in the conduction orbital at site j. The first terms on the right-hand side are the effective one-electron energies, having the form $H_{i'i'}(\text{size}) \approx h_{a_{i'}a_{i'}} + 2\sum_{j\neq i}(a_i'a_i'|a_ja_j)$. The orbital energy differences are raised by repulsions due to the presence of electrons on nearby sites, hence providing the primary origin of quantum size effects. That is, quantum size effects increase the zeroth-order energy gaps (and thus the band gap) as the size of the system diminishes, which is indicated explicitly in eqs 5a and 5b by the notation "(size)". That effect is well-known for molecules and various nanoscale systems.[2,79,115–117] Importantly, it is evident that the primary quantum size effect is to increase the band gap (*i.e.*, the difference between ionization potential and electron affinity) and, as a consequence, the exciton transition energy as seen in the absorption spectrum. It should be noted that the energies of unoccupied orbitals are highly overestimated by Hartree–Fock calculations because the orbital energies are obtained on the basis of the effective field of the ground-state electronic configuration. Thus, electron relaxation and correlation effects are ignored, which are the same approximations assumed in Koopmans's theorem.[118]

The excitation energy, before singlet–triplet splitting, of site i is written E_0^i.The exchange integral $J_0^i = (a_i'a_i|a_ia_i')$ determines the singlet–triplet splitting of site i in isolation. EA_i and IP_i designate electron affinity and ionization potential of the subunit at site i, respectively (defining the zeroth-order gap mentioned later). The repulsion term $C_0^j = 2(a_j'a_j'|a_ja_j) - (a_ja_j|a_ja_j) - J_0^j$ raises the energy of the CT configuration to equal that of a free carrier state.[74] The final term in eq 5b, $C_{ij} = (a_ia_i|a_j'a_j')$ is the electron–hole attraction. This term lowers the energy of each CT configuration according to the electron–hole separation, yielding a Rydberg-like series of zeroth-order energy levels. The polarization effects[119] can be included *via* the energy shift terms P_{LE} and P_{CT}.[120]

To obtain the nanoscale exciton states α in terms of the mixing coefficients λ_r^α, the secular eqs 6 were solved,

$$\sum_s (H_{rs} - E_\alpha S_{rs})\lambda_s^\alpha = 0 \quad (6)$$

where the energies E_α are defined relative to the ground-state energy of the aggregate, E_0, matrix elements are $H_{rs} = \langle\psi_s|H - E_0|\psi_r\rangle$ and the overlap integrals are $S_{rs} = \langle\psi_s|\psi_r\rangle$. Thus, the exciton states of eq 7 are obtained as linear combinations of the LE and CT configurations:

$$\Psi_\alpha = \sum_s \lambda_s^\alpha \psi_s \quad (7)$$

Here we calculate the lowest singlet exciton manifold only. Higher exciton states can be found by including more subunit orbitals in the construction of the CSFs, eqs 4a and 4b. Note that the excited states obtained using eq 6 are equivalent to those obtained by forming the molecular orbitals (Figure 2d) and then undertaking a configuration interaction calculation using all single excitations from the Hartree–Fock reference determinant.[121] Higher-order approximations can be built systematically into this model,[122] and such electron correlation effects are known to be important corrections to the basic theory.[123]

The transition dipole moment of eigenstate Ψ_α is the linear combination

$$\vec{\mu}_{0\alpha} = \sum_s \lambda_s^\alpha \vec{\mu}_{0s} \quad (8)$$

where $\vec{\mu}_{0s} = -S_{ij}\vec{\mu}_{0j}$ for the configuration s that consists of a hole at site i and an electron at site j. The explicit dependence of this quantity on the overlap integral $S_{ij} = \langle a_j|a_i\rangle$ shows why CTXs—those states comprised primary of CT configurations—carry negligible transition dipole strength compared to Frenkel excitons. In Frenkel excitons, the electron and hole are localized to the same subunits, so $S_{ij} = 1$. As the electron–hole separation increases in the set of CT configurations, S_{ij} diminishes exponentially. Similar arguments confirm that the CTX states are not two-photon-allowed either.

The *static* dipole moment $\vec{\mu}_\alpha \approx \sum_s e(\mathbf{r}_j - \mathbf{r}_i)_s(\lambda_s^\alpha)^2$ of each excited state α in our model calculations for a homogeneous system is zero owing to symmetry. However, an average electron–hole pair separation, eq 9, can be defined for each eigenstate, and this quantity signals the extent of CT character in that wave function:

$$R_{e-h}^\alpha \approx \sum_s |(\mathbf{r}_j - \mathbf{r}_i)_s|(\lambda_s^\alpha)^2 \quad (9)$$

This quantity is not a definition of exciton size; rather, it indicates the CT character of the density of states as a function of energy. Exciton size, or coherence size, can be defined in a number of different ways, including the inverse participation ratio, width of the distribution of orbital coefficients in the wave function, density matrix, or root-mean-square electron–hole separation.[47,124–127] Exciton size is not explicitly considered in the present work.

Model example calculations based on this theory are reported. Parameters were chosen to provide general insights into the electronic structure of nanoscale excitons, rather than attempting to model any specific systems. Note that quantitative calculations of materials,[128–134] like those for simple molecular systems,[135] require the application of much more sophisticated methods. Spectra were calculated by assuming that each exciton state is weakly coupled to a phonon bath that is represented as an overdamped Brownian oscillator.[136] The temperature was set to 1 K.

Acknowledgment. The Natural Sciences and Engineering Research Council of Canada is gratefully acknowledged for support of this research. I acknowledge the support of an E. W. R. Steacie Memorial Fellowship and thank G. Rumbles for inspiring discussions.

APPENDIX

It is clear that the theory developed in the Methods section applies to molecular assemblies. Here it will be established how that theory can also apply to bonded systems (molecular or nanoscale) where the definition of distinct subunits, and hence

TABLE 1. Chirgwin–Coulson Weights Calculated for VB Structures I–VI in the Ground and First Excited Singlet States of Ethene

structure	ground state	excited state
I	0.062	0.471
II	0.062	0.471
III	0.069	0.029
IV	0.069	0.029
V	0.798	0.00
VI	−0.060	0.00

LE configurations, is unclear. To see the connection, it is first necessary to point out that the model described in Figure 2 is a mixed molecular orbital (MO)–valence bond (VB) representation, because the LE configurations are drawn in the MO representation. However, the model can be generalized for any system by using a fully VB representation. To see how that works, in this Appendix the VB description of excited states is discussed, since this theory is not widely known.

Ab initio VB calculations provide useful insights into the relationship between charge-transfer configurations and electronic excited states. Illustrative calculations of the ground and first excited singlet states of ethane (ground-state geometry) obtained using an *ab initio* VB method[137] and STO-6G basis set (with orbital exponents and hybridization independently optimized for ground and excited states) will be summarized here. The results of these four-electron calculations are part of a more detailed study including all electrons and many more VB structures (G. D. Scholes and R. D. Harcourt, unpublished). The $2p_z$ orbital on each carbon center forms the π bond, while an sp^2 hybrid orbital on each center forms the σ bond. The VB structures **I**–**VI** in Chart 1 were explicitly considered. In Table 1, the Chirgwin–Coulson weights obtained for each structure in the ground- and excited-state wave functions are compared. Of course, the π-bond (**V**) dominates the ground state, but notice the general result that the ionic structures (**I**, **II**) dominate the first excited state. Thus, in the VB picture, the locally excited state is represented as a resonance between ionic configurations.

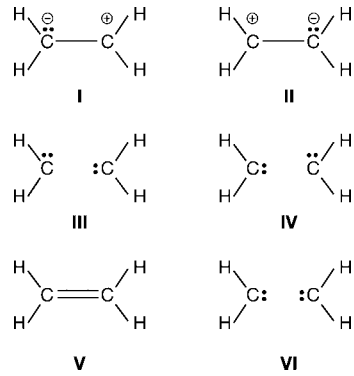

Chart 1. Valence bond structures I–VI

As the π system is extended, for example to 1,3-butadiene,[73] it is found that nearest-neighbor CT (ionic) configurations dominate the composition of the first excited state, while more separated electron–hole pairs contribute with lower weight. This allows the connection with the Hamiltonian of eq 3, such that the resonance structures among nearest-neighbor CT configurations can be collectively relabeled the LE configurations (since they are the primary excited states), while the more extended CT components of the wave function contribute to the CT block. Developing this model in further detail will be the subject of future work.

REFERENCES AND NOTES

1. Duan, X.; Huang, Y.; Wang, J.; Lieber, C. M. Indium Phosphide Nanowires as Building Blocks for Nanoscale Electronic and Optoelectronic Devices. *Nature* **2001**, *409*, 66–69.
2. Scholes, G. D.; Rumbles, G. Excitons in Nanoscale Systems. *Nat. Mater.* **2006**, *5*, 683–696.
3. Sirringhaus, H.; Brown, P. J.; Friend, R. H.; Nielsen, M. M.; Bechgaard, K.; Langeveld-Voss, B. M. W.; Spiering, A. J. H.; Janssen, R. A. J.; Meijer, E. W.; Herwig, P.; de Leeuw, D. M. Two-Dimensional Charge Transport in Self-Organized, High-Mobility Conjugated Polymers. *Nature* **1999**, *401*, 685–688.
4. Gregg, B. A. Excitonic Solar Cells. *J. Phys. Chem. B* **2003**, *107*, 4688–4698.
5. Konstantatos, G.; Howard, I.; Fischer, A.; Hoogland, S.; Clifford, J.; Klem, E.; Levina, L.; Sargent, E. H. Ultrasensitive Solution-Cast Quantum Dot Photodetectors. *Nature* **2006**, *442*, 180–183.
6. Klimov, V. I.; Ivanov, S. A.; Nanda, J.; Achermann, M.; Bezel, I.; McGuire, J. A.; Piryatinski, A. Single-Exciton Optical Gain in Semiconductor Nanocrystals. *Nature* **2007**, *447*, 441–446.
7. Marder, S. R.; Kippelen, B.; Jen, A. K.-Y.; Peyghambarian, N. Design and Synthesis of Chromophores and Polymers for Electro-Optic and Photorefractive Applications. *Nature* **1997**, *388*, 845–851.
8. Swager, T. M. The Molecular Wire Approach to Sensory Signal Amplification. *Acc. Chem. Res.* **1998**, *31*, 201–207.
9. Wang, L. W.; Zunger, A. High-Energy Excitonic Transitions in Cdse Quantum Dots. *J. Phys. Chem. B* **1998**, *102*, 6449–6454.
10. Koch, E. E.; Otto, A. Optical Absorption of Benzene Vapour for Photon Energies from 6 eV to 35 eV. *Chem. Phys. Lett.* **1972**, *12*, 476–480.
11. Robin, M. B. *Higher Excited States of Polyatomic Molecules*; Academic Press: New York and London, 1974; Vol. 1.
12. Slater, J. C.; Shockley, W. Optical Absorption by the Alkali Halides. *Phys. Rev.* **1936**, *50*, 705–719.
13. Azumi, T.; Armstrong, A. T.; McGlynn, S. P. Energy of Excimer Luminescence. II. Configuration Interaction between Molecular Exciton States and Charge Resonance States. *J. Chem. Phys.* **1964**, *41*, 3839–3852.
14. Murrell, J. N.; Tanaka, J. The Theory of the Electronic Spectra of Aromatic Hydrocarbon Dimers. *Mol. Phys.* **1964**, *7*, 363–380.
15. Bittner, E. R.; Karabunarliev, S. Energy Relaxation Dynamics and Universal Scaling Laws in Organic Light-Emitting Diodes. *Int. J. Quantum Chem.* **2003**, *95*, 521–531.
16. Köhler, A.; dos Santos, D. A.; Beljonne, D.; Shuai, Z.; Brédas, J.-L.; Holmes, A. B.; Kraus, A.; Müllen, K.; Friend, R. H. Charge Separation in Localized and Delocalized Electronic States in Polymeric Semiconductors. *Nature* **1998**, *392*, 903–906.
17. Jespersen, K. G.; Beenken, W. J. D.; Zaushitsyn, Y.; Yartsev, A.; Andersson, M.; Pullerits, T.; Sundström, V. The Electronic States of Polyfluorene Copolymers with Alternating Donor-Acceptor Units. *J. Chem. Phys.* **2004**, *121*, 12613–12617.
18. Bittner, E. R. Lattice Theory of Ultrafast Excitonic and Charge-Transfer Dynamics in DNA. *J. Chem. Phys.* **2006**, *125*, 094909.
19. Knupfer, M.; Schwieger, T.; Peisert, H.; Fink, J. Mixing of Frenkel and Charge Transfer Excitons in Quasi-One-Dimensional Copper Phthalocyanine Molecular Crystals. *Phys. Rev. B* **2004**, *69*, 165210.
20. Lanzani, G.; Frolov, S. V.; Lane, P. A.; Vardeny, Z. V.; Nisoli, M.; De Silvestri, S. Transient Spectroscopy of Frenkel and Charge Transfer Excitons in a-Sexithienyl Films. *Phys. Rev. Lett.* **1997**, *79*, 3066–3069.
21. Andrzejak, M.; Petelenz, P.; Slawik, M.; Munn, R. W. Theoretical Calculation of the Electro-Absorption Spectrum of the S-Sexithiophene Single Crystal. *J. Chem. Phys.* **2002**, *117*, 1328–1335.
22. Rochefort, A.; Boyer, P.; Nacer, B. Resonant Tunneling Transport in Highly Organized Oligoacene Assemblies. *Org. Electron.* **2007**, *8*, 1–7.

23. Bittner, E. R.; Karabunarliev, S.; Ye, A. Photoconductivity and Current Producing States in Molecular Semiconductors. *J. Chem. Phys.* **2005**, *122*, 034707.
24. Monshouwer, R.; Abrahamsson, M.; van Mourik, F.; van Grondelle, R. Superradiance and Exciton Delocalization in Bacterial Photosynthetic Light-Harvesting Systems. *J. Phys. Chem. B* **1997**, *101*, 7241–7248.
25. Dahlbom, M.; Pullerits, T.; Mukamel, S.; Sundström, V. Exciton Delocalization in the B850 Light-Harvesting Complex: Comparison of Different Measures. *J. Phys. Chem. B* **2001**, *105*, 5515–5524.
26. Bakalis, L. D.; Knoester, J. Pump-Probe Spectroscopy and the Exciton Delocalization Length in Molecular Aggregates. *J. Phys. Chem. B* **1999**, *103*, 6620–6628.
27. Leng, J. M.; Jeglinski, S.; Wei, X.; Benner, R. E.; Vardeny, Z. V.; Guo, F.; Mazumdar, S. Optical Probes of Excited States in Poly(p-Phenylenevinylene). *Phys. Rev. Lett.* **1994**, *72*, 156–159.
28. Brédas, J. L.; Cornil, J.; Heeger, A. J. The Exciton Binding Energy in Luminescent Conjugated Polymers. *Adv. Mater.* **1996**, *8*, 447–452.
29. Moses, D.; Wang, J.; Heeger, A. J.; Kirova, N.; Brazovski, S. Singlet Exciton Binding Energy in Poly(Phenylene Vinylene). *Proc. Natl. Acad. Sci.* **2001**, *98*, 13496–13500.
30. Arkhipov, V. I.; Bässler, H. Exciton Dissociation and Charge Photogeneration in Pristine and Doped Conjugated Polymers. *Phys. Stat. Solidi (a)* **2004**, *201*, 1152–1187.
31. Silva, C.; Russell, D. M.; Dhoot, A. S.; Herz, L. M.; Daniel, C.; Greenham, N. C.; Arias, A. C.; Setayesh, S.; Müllen, K.; Friend, R. H. Exciton and Polaron Dynamics in a Step-Ladder Polymeric Semiconductor: The Influence of Interchain Order. *J. Phys.: Condens. Matter* **2002**, *14*, 9803–9824.
32. Korovyanko, O. J.; Österbacka, R.; Jiang, X. M.; Vardeny, Z. V.; Janssen, R. A. J. Photoexcitation Dynamics in Regioregular and Regiorandom Polythiophene Films. *Phys. Rev. B* **2001**, *64*, 235122.
33. Dicker, G.; de Haas, M. P.; Siebbeles, L. D. A.; Warman, J. M. Electrodeless Time-Resolved Microwave Conductivity Study of Charge-Carrier Photogeneration in Regioregular Poly(3-Hexylthiophene) Thin Films. *Phys. Rev. B* **2004**, *70*, 045203.
34. Wang, F.; Dukovic, G.; Brus, L. E.; Heinz, T. F. The Optical Resonances in Carbon Nanotubes Arise from Excitons. *Science* **2005**, *308*, 838–841.
35. Scheblykin, I. G.; Yartsev, A.; Pullerits, T.; Gulbinas, V.; Sundström, V. Excited State and Charge Photogeneration Dynamics in Conjugated Polymers. *J. Phys. Chem. B* **2007**, *111*, 6303–6321.
36. Ma, Y.-Z.; Valkunas, L.; Bachilo, S. M.; Fleming, G. R. Exciton Binding Energy in Semiconducting Single-Walled Carbon Nanotubes. *J. Phys. Chem. B* **2005**, *109*, 15671–15674.
37. Zhao, H.; Mazumdar, S. Electron-Electron Interaction Effects on the Optical Excitations of Semiconducting Single-Walled Carbon Nanotubes. *Phys. Rev. Lett.* **2004**, *93*, 157402.
38. Spataru, C. D.; Ismail-Beigi, S.; Benedict, L. X.; Louie, S. G. Excitonic Effects and Optical Spectra of Single-Walled Carbon Nanotubes. *Phys. Rev. Lett.* **2004**, *92*, 77402.
39. Knox, R. S., Introduction to Exciton Physics. In *Collective Excitations in Solids*; Bartolo, B. D., Ed.; Plenum Press: New York and London, 1981; pp 183–245..
40. Hoffmann, R. How Chemistry Meets Physics in the Solid State. *Angew. Chem., Int. Ed. Engl.* **1987**, *26*, 846–878.
41. Basu, P. K., *Theory of the Optical Processes in Semiconductors: Bulk and Microstructures*; Oxford University Press: New York, 1997.
42. Kuper, C. G.; Whitfield, G. D. *Polarons and Excitons—Scottish Universities' Summer School*; Plenum Press: New York, 1962.
43. Nelson, J. *The Physics of Solar Cells*; Imperial College Press: London, 2003.
44. McRae, E. G.; Kasha, M. The Molecular Exciton Model. *Physical Processes in Radiation Biology*; Academic Press: New York, 1964; pp 23–42..
45. Scholes, G. D.; Ghiggino, K. P. Electronic Interactions and Interchromophore Energy Transfer. *J. Phys. Chem.* **1994**, *98*, 4580–4590.
46. Dexter, D. L. A Theory of Sensitized Luminescence in Solids. *J. Chem. Phys.* **1953**, *21*, 836–850.
47. Fidder, H.; Knoester, J.; Wiersma, D. A. Optical Properties of Disorder Molecular Aggregates: A Numerical Study. *J. Chem. Phys.* **1991**, *95*, 7880–7890.
48. Chernyak, V.; Mukamel, S. Collective Coordinates for Nuclear Spectral Densities in Energy Transfer and Femtosecond Spectroscopy of Molecular Aggregates. *J. Chem. Phys.* **1996**, *105*, 4565–4583.
49. Freiberg, A.; Rätsep, M.; Timpmann, K.; Trinkunas, G.; Woodbury, N. Self-Trapped Excitons in LH2 Antenna Complexes between 5 K and Ambient Temperature. *J. Phys. Chem. B* **2003**, *107*, 11510–11519.
50. Tretiak, S.; Kilina, S.; Piryatinski, A.; Saxena, A.; Martin, A. L.; Bishop, A. R. Excitons and Peierls Distortion in Conjugated Carbon Nanotubes. *Nano Lett.* **2007**, *7*, 86–92.
51. Dahlbom, M.; Beenken, W.; Sundström, V.; Pullerits, T. Collective Excitation Dynamics and Polaron Formation in Molecular Aggregates. *Chem. Phys. Lett.* **2002**, *364*, 556–561.
52. Yencha, A. J.; Hall, R. I.; Avaldi, L.; Dawber, G.; McConkey, A. G.; MacDonald, M. A.; King, G. C. Threshold Photoelectron Spectroscopy of Benzene up to 26.5 eV. *Can. J. Chem.* **2004**, *82*, 1061–1066.
53. Craig, D. P.; Walmsley, S. H. *Excitons in Molecular Crystals; Theory and Applications*; Benjamin: New York, 1968.
54. Löwdin, P.-O. Quantum Theory of Nonmetallic Crystals. *J. Appl. Phys.* **1962**, *33*, 251–280.
55. Coulson, C. A. *Valence*; Clarendon Press: Oxford, 1952.
56. Cooper, D. L.; Gerratt, J.; Raimondi, M. Applications of Spin-Coupled Valence Bond Theory. *Chem. Rev.* **1991**, *91*, 929–964.
57. Löwdin, P.-O. On the Historical Development of the Valence Bond Method and the Non-Orthogonality Problem. *J. Mol. Struct. (Theochem)* **1991**, *229*, 1–14.
58. Chandross, M.; Shimoi, Y.; Mazumdar, S. Diagrammatic Exciton-Basis Valence-Bond Theory of Linear Polyenes. *Phys. Rev. B* **1999**, *59*, 4822–4838.
59. Blinov, L. M.; Palto, S. P.; Ruani, G.; Taliani, C.; Tevosov, A. A.; Yudin, S. G.; Zamboni, R. Location of Charge Transfer States in α-Sexithienyl Determined by the Electroabsorption Technique. *Chem. Phys. Lett.* **1995**, *232*, 401–406.
60. Petelenz, P. Charge-Transfer Interactions—Their Manifestations in Electroabsorption Spectra. *J. Lumin.* **2004**, *110*, 325–331.
61. Berry, R. S.; Jortner, J.; Mackie, J. C.; Pysh, E. S.; Rice, S. A. Search for a Charge-Transfer State in Crystalline Anthracene. *J. Chem. Phys.* **1965**, *42*, 1535–1540.
62. Najafov, H.; Biaggio, I.; Podzorov, V.; Calhoun, M. F.; Gershenson, M. E. Primary Photoexcitations and the Origin of the Photocurrent in Rubrene Single Crystals. *Phys. Rev. Lett.* **2006**, *96*, 056604.
63. Bounds, P. J.; Petelenz, P.; Siebrand, W. Charge-Transfer Excitons in Anthracene Crystals. A Theoretical Investigation of Their Optical Absorption and Thermal Dissociation. *Chem. Phys.* **1981**, *63*, 303–320.
64. Choi, S.-I.; Jortner, J.; Rice, S. A.; Silbey, R. Charge-Transfer Exciton States in Aromatic Molecular Crystals. *J. Chem. Phys.* **1964**, *41*, 3294–3306.
65. Ohno, K. Some Remarks on the Pariser-Parr-Pople Method. *Theor. Chim. Acta* **1964**, *2*, 219–227.
66. Mataga, N. Electronic Structure and Spectra of S-Tetrazine. *Bull. Chem. Soc. Jpn.* **1958**, *31*, 453–458.
67. Mulliken, R. S. Molecular Compounds and Their Spectra. II. *J. Am. Chem. Soc.* **1952**, *74*, 811–824.
68. Chandross, M.; Mazumdar, S.; Jeglinski, S.; Wei, X.; Vardeny, Z. V.; Kwock, E. W.; Miller, T. M. Excitons in Poly(Para-Phenylenevinylene). *Phys. Rev. B* **1994**, *50*, R14702–14705.
69. Brédas, J. L.; Calbert, J. P.; da Silva, D. A.; Cornil, J. Organic Semiconductors: A Theoretical Characterization of the

Basic Parameters Governing Charge Transport. *Proc. Natl. Acad. Sci. U.S.A.* **2002**, *99*, 5804–5809.
70. Fanceschetti, A.; Zunger, A. Direct Pseudopotential Calculation of Exciton Coulomb and Exchange Energies in Semiconductor Quantum Dots. *Phys. Rev. Lett.* **1997**, *78*, 915–918.
71. Wang, Z.; Zhao, H.; Mazumdar, S. Quantitative Calculations of the Excitonic Energy Spectra of Semiconducting Single-Walled Carbon Nanotubes within a Pi-Electron Model. *Phys. Rev. B* **2006**, *74*, 195406.
72. Harcourt, R. D. Valence Bond Studies of O_2 and O_2^-: A Note on One-Electron and Two-Electron Transfer Resonances. *J. Phys. Chem.* **1992**, *96*, 7616–7619.
73. Bachler, V.; Schaffner, K. The Photochemistry of 1,3-Butadiene Rationalized by Means of Theoretical Resonance Structures and Their Weights. *Chem. Eur. J.* **2000**, *6*, 959–970.
74. Scholes, G. D.; Harcourt, R. D.; Ghiggino, K. P. Rate Expressions for Excitation Transfer: III, an Ab Initio Study of Electronic Factors in Excitation Transfer and Exciton Resonance Interactions. *J. Chem. Phys.* **1995**, *102*, 9574–9581.
75. Bir, G. L.; Pikus, G. E. *Symmetry and Strain-Induced Effects in Semiconductors*; Wiley: New York, 1975.
76. Efros, A. L.; Rosen, M.; Kuno, M.; Nirmal, M.; Norris, D. J.; Bawendi, M. G. Band-Edge Exciton in Quantum Dots of Semiconductors with a Degenerate Valence Band: Dark and Bright Exciton States. *Phys. Rev. B* **1996**, *54*, 4843–4856.
77. Scholes, G. D.; Kim, J.; Wong, C. Y. Exciton Spin Relaxation in Quantum Dots Measured Using Ultrafast Transient Polarization Grating Spectroscopy. *Phys. Rev. B* **2006**, *73*, 195325.
78. Barford, W. Theory of Singlet Exciton Yield in Light-Emitting Polymers. *Phys. Rev. B* **2004**, *70*, 205204.
79. Klevens, H. B.; Platt, J. R. Spectral Resemblances of Cata-Condensed Hydrocarbons. *J. Chem. Phys.* **1949**, *17*, 470–481.
80. Platt, J. R. Classification of Spectra of Cata-Condensed Hydrocarbons. *J. Chem. Phys.* **1949**, *17*, 484–495.
81. Clar, E.; Zander, M. Aromatische Kohlenwasserstoffe, LXXII. *Chem. Ber.* **1956**, *89*, 749–762.
82. McGlynn, S. P.; Azumi, T.; Kinoshita, M. *Molecular Spectroscopy of the Triplet State*; Prentice-Hall: Englewood Cliffs, NJ, 1969.
83. Harcourt, R. D.; Scholes, G. D.; Ghiggino, K. P. Rate Expressions for Excitation Transfer: II. Electronic Considerations of Direct and through-Configuration Exciton Resonance Interactions. *J. Chem. Phys.* **1994**, *101*, 10521–10525.
84. Mortimer, I. B.; Nicholas, R. J. Role of Bright and Dark Excitons in the Temperature-Dependent Photoluminscence of Carbon Nanotubes. *Phys. Rev. Lett.* **2007**, *98*, 027404.
85. Perebeinos, V.; Tersoff, J.; Avouris, P. Radiative Lifetime of Excitons in Carbon Nanotubes. *Nano Lett.* **2005**, *5*, 2495–2499.
86. Scholes, G. D.; Tretiak, S.; McDonald, T. J.; Metzger, W. K.; Engtrakul, C.; Rumbles, G.; Heben, M. J. Low-Lying Exciton States Determine the Photophysics of Semiconducting Single Wall Carbon Nanotubes. *J. Phys. Chem. C* **2007**, *111*, 11139–11149.
87. Miller, P. F.; deSouza, M. M.; Moratti, S. C.; Holmes, A. B.; Samuel, I. D. W.; Rumbles, G. The Equilibrium of Intrachain and Interchain Excitations in Aggregates of a Cyano-Substituted Phenylene Vinylene Polymer. *Polym. Int.* **2006**, *55*, 784–792.
88. Kiowski, O.; Arnold, K.; Lebedkin, S.; Hennrich, F.; Kappes, M. M. Direct Observation of Deep Excitonic States in the Photoluminescence Spectra of Single-Walled Carbon Nanotubes. *Phys. Rev. Lett.* **2007**, *99*, 237402.
89. Cogdell, R. J.; Gall, A.; Köhler, J. The Architecture and Function of the Light-Harvesting Apparatus of Purple Bacteria: From Single Molecules to in Vivo Membranes. *Q. Rev. Biophys.* **2006**, *39*, 227–324.
90. Scholes, G. D.; Curutchet, C.; Mennucci, B.; Cammi, R.; Tomasi, J. How Solvent Controls Electronic Energy Transfer and Light Harvesting. *J. Phys. Chem. B* **2007**, *111*, 6978–6982.
91. Wang, L.-W.; Zunger, A. Dielectric Constants of Silicon Quantum Dots. *Phys. Rev. Lett.* **1994**, *73*, 1039–1042.
92. Pope, M.; Swenberg, C. E. Electronic Processes in Organic Solids. *Annu. Rev. Phys. Chem.* **1984**, *35*, 613–655.
93. Chen, T.-A.; Wu, X.; Rieke, R. D. Regiocontrolled Synthesis of Poly(3-Alkylthiophenes) Mediated by Rieke Zinc: Their Characterization and Solid-State Properties. *J. Am. Chem. Soc.* **1995**, *117*, 233–244.
94. Österbacka, R.; An, C. P.; Jiang, X. M.; Vardeny, Z. V. Two-Dimensional Electronic Excitations in Self-Assembled Conjugated Polymer Nanocrystals. *Science* **2000**, *287*, 839–842.
95. Wang, X.; Dykstra, T. E.; Scholes, G. D. Photon-Echo Studies of Collective Absorption and Dynamic Localization of Excitation in Conjugated Polymers and Oligomers. *Phys. Rev. B* **2005**, *71*, 45203.
96. Yaliraki, S. N.; Silbey, R. J. Conformational Disorder of Conjugated Polymers: Implications for Optical Properties. *J. Chem. Phys.* **1996**, *104*, 1245–1253.
97. Kohler, B. E.; Samuel, I. D. W. Experimental Determination of Conjugation Lengths in Long Polyene Chains. *J. Chem. Phys.* **1995**, *103*, 6248–6252.
98. Bässler, H.; Schweitzer, B. Site-Selective Fluorescence Spectroscopy of Conjugated Polymers and Oligomers. *Acc. Chem. Res.* **1999**, *32*, 173–182.
99. Spataru, C. D.; Ismail-Beigi, S.; Capaz, R. B.; Louie, S. G. Theory and Ab Initio Calculation of the Radiative Lifetime of Excitons in Semiconducting Carbon Nanotubes. *Phys. Rev. Lett.* **2005**, *95*, 247402.
100. Bednarz, M.; Malyshev, V. A.; Knoester, J. Temperature Dependent Fluorescence in Disordered Frenkel Chains: Interplay of Equilibrium and Local Band-Edge Level Structure. *Phys. Rev. Lett.* **2003**, *91*, 217401.
101. Wang, L. W.; Califano, M.; Zunger, A.; Franceschetti, A. Pseudopotential Theory of Auger Processes in Cdse Quantum Dots. *Phys. Rev. Lett.* **2003**, *91*, 056404.
102. Klimov, V. I. Spectral and Dynamical Properties of Multilexcitons in Semiconductor Nanocrystals. *Annu. Rev. Phys. Chem.* **2007**, *58*, 635–673.
103. Bittner, E. R.; Ramon, J. G. S.; Karabunarliev, S. Exciton Dissociation Dynamics in Model Donor-Acceptor Polymer Heterojunctions. I. Energetics and Spectra. *J. Chem. Phys.* **2005**, *122*, 214719.
104. Morteani, A. C.; Dhoot, A. S.; Kim, J.-S.; Silva, C.; Greenham, N. C.; Murphy, C.; Moons, E.; Ciná, S.; Burroughs, J. H.; Friend, R. H. Barrier-Free Electron-Hole Capture in Polymer Blend Heterojunction Light-Emitting Diodes. *Adv. Mater.* **2003**, *15*, 1708–1712.
105. Sariciftci, N. S.; Smilowitz, L.; Heeger, A. J.; Wudl, F. Photoinduced Electron Transfer from a Conducting Polymer to Buckminsterfullerene. *Science* **1992**, *258*, 1474–1476.
106. Tamura, H.; Bittner, E. R.; Burghardt, I. Exciton Dissociation at Donor-Acceptor Polymer Heterojunctions: Quantum Nonadiabatic Dynamics and Effective-Mode Analysis. *J. Chem. Phys.* **2007**, *126*, 021103.
107. Krueger, B. P.; Scholes, G. D.; Fleming, G. R. Calculation of Couplings and Energy Transfer Pathways between the Pigments of Lh2 by the Ab Initio Transition Density Cube Method. *J. Phys. Chem. B* **1998**, *102*, 5378–5386.
108. Scholes, G. D. Long-Range Resonance Energy Transfer in Molecular Systems. *Annu. Rev. Phys. Chem.* **2003**, *54*, 57–87.
109. Wong, K. F.; Bagchi, B.; Rossky, P. J. Distance and Orientation Dependence of Excitation Transfer Rates in Conjugated Systems: Beyond the Forster Theory. *J. Phys. Chem. A* **2004**, *108*, 5752–5763.
110. Beljonne, D.; Pourtois, G.; Silva, C.; Hennebicq, E.; Herz, L. M.; Friend, R. H.; Scholes, G. D.; Setayesh, S.; Müllen, K.;

Brédas, J. L. Interchain Vs. Intrachain Energy Transfer in Acceptor-Capped Conjugated Polymers. *Proc. Natl. Acad. Sci. U.S.A.* **2002**, *99*, 10982–10987.
111. Beenken, W. J. D.; Pullerits, T. Excitonic Coupling in Polythiophenes: Comparison of Different Calculation Methods. *J. Chem. Phys.* **2004**, *120*, 2490–2495.
112. Newton, M. D. Quantum Chemical Probes of Electron-Transfer Kinetics: The Nature of Donor-Acceptor Interactions. *Chem. Rev.* **1991**, *91*, 767–792.
113. Coropceanu, V.; Cornil, J.; da Silva, D. A.; Olivier, Y.; Silbey, R.; Brédas, J. L. Charge Transport in Organic Semiconductors. *Chem. Rev.* **2007**, *107*, 926–952.
114. McWeeny, R. *Methods of Molecular Quantum Mechanics*, 2nd ed.; Academic Press: London, 1992.
115. Ekimov, A. I.; Hache, F.; Schanne-Klein, M. C.; Ricard, D.; Flytzanis, C.; Kudryavtsev, I. A.; Yazeva, T. V.; Rodina, A. V.; Efros, A. L. Absorption and Intensity-Dependent Photoluminescence Measurement on CdSe Quantum Dots: Assignment of the First Electronic Transitions. *J. Opt. Soc. Am. B* **1993**, *10*, 100–107.
116. Banin, U.; Millo, O. Tunneling and Optical Spectroscopy of Semiconductor Nanocrystals. *Annu. Rev. Phys. Chem.* **2003**, *54*, 465–492.
117. Bachilo, S. M.; Strano, M. S.; Kittrell, C.; Hauge, R. H.; Smalley, R. E.; Weisman, R. B. Structure-Assigned Optical Spectra of Single-Walled Carbon Nanotubes. *Science* **2002**, *298*, 2361–2366.
118. Hinchliffe, A. *Ab Initio Determination of Molecular Properties*; Adam Hilger: Bristol, 1987.
119. Andrzejak, M.; Petelenz, P. Polarization Energy Calculations of Charge Transfer States in the a-Sexithiophene Crystal. *Synth. Met.* **2000**, *109*, 97–100.
120. Suppan, P. Solvatochromic Shifts: The Influence of the Medium on the Energy of Electronic States. *J. Photochem. Photobiol. A: Chem.* **1990**, *50*, 293–330.
121. Scholes, G. D.; Harcourt, R. D.; Fleming, G. R. Electronic Interactions in Photosynthetic Light-Harvesting Complexes: The Role of Carotenoids. *J. Phys. Chem. B* **1997**, *101*, 7302–7312.
122. Scholes, G. D.; Harcourt, R. D. Configuration Interaction and the Theory of Columbic Interactions in Energy Transfer and Molecular Exciton Interactions. *J. Chem. Phys.* **1996**, *104*, 5054–5061.
123. Igumenshchev, K. I.; Tretiak, S.; Chernyak, V. Y. Excitonic Effects in a Time-Dependent Density Functional Theory. *J. Chem. Phys.* **2007**, *127*, 114902.
124. Meier, T.; Zhao, Y.; Chernyak, V. Y.; Mukamel, S. Polarons, Localization, and Excitonic Coherence in Superradiance of Biological Antenna Complexes. *J. Chem. Phys.* **1997**, *107*, 3876–3893.
125. Tretiak, S.; Chernyak, V.; Mukamel, S. Two-Dimensional Real-Space Analysis of Optical Excitations in Acceptor-Substituted Carotenoids. *J. Am. Chem. Soc.* **1997**, *119*, 11408–11419.
126. Hennebicq, E.; Deleener, C.; Brédas, J. L.; Scholes, G. D.; Beljonne, D. Chromophores in Phenylenevinylene-Based Conjugated Polymers: Role of Conformational Kinks and Chemical Defects. *J. Chem. Phys.* **2006**, *125*, 054901.
127. Perebeinos, V.; Tersoff, J.; Avouris, P. Scaling of Excitons in Carbon Nanotubes. *Phys. Rev. Lett.* **2004**, *92*, 257402.
128. Cohen, M. L. The Theory of Real Materials. *Annu. Rev. Mater. Sci.* **2000**, *30*, 1–26.
129. Rohlfing, M.; Louie, S. G. Electron-Hole Excitations and Optical Spectra from First Principles. *Phys. Rev. B* **2000**, *62*, 4927–4944.
130. Schatz, G. C. Using Theory and Computation to Model Nanoscale Properties. *Proc. Natl. Acad. Sci. U.S.A.* **2007**, *104*, 6885–6892.
131. Brédas, J.-L.; Cornil, J.; Beljonne, D.; dos Santos, D. A.; Shuai, Z. Excited-State Electronic Structure of Conjugated Oligomers and Polymers: A Quantum-Chemical Approach to Optical Phenomena. *Acc. Chem. Res.* **1999**, *32*, 267–276.
132. Franceschetti, A.; Fu, H.; Wang, L. W.; Zunger, A. Many-Body Pseudopotential Theory of Excitons in Inp and Cdse Quantum Dots. *Phys. Rev. B* **1999**, *60*, 1819–1829.
133. Zhao, H.; Mazumdar, S.; Sheng, C. X.; Tong, M.; Vardeny, Z. V. Photophysics of Excitons in Quasi-One-Dimensional Organic Semiconductors: Single-Walled Carbon Nanotubes and Pi-Conjugated Polymers. *Phys. Rev. B* **2006**, *73*, 075403.
134. Abolfath, R. M.; Hawrylak, P. Real Space Hartree-Fock Configuration Interaction Method for Complex Lateral Quantum Dot Molecules. *J. Chem. Phys.* **2006**, *125*, 034707.
135. McWeeny, R. On the Nature of the Oxygen Double Bond. *J. Mol. Struct. (Theochem)* **1991**, *229*, 29–38.
136. Mukamel, S. *Principles of Nonlinear Optical Spectroscopy*; Oxford University Press: New York, 1995.
137. Harcourt, R. D.; Roso, W. Valence-Bond Studies of 4-Electron 3-Center Bonding Units. 1. Pi-Electrons of O^-_3, NO_2^-, and CH_2N_2. *Can. J. Chem.* **1978**, *56*, 1093–1101.